References and Notes

1. A. S. Kondrashov, *J. Hered.* **84**, 372 (1993).
2. H. J. Muller, *Mutat. Res.* **1**, 2 (1964).
3. M. Kimura and T. Maruyama, *Genetics* **54**, 1337 (1966).
4. B. Charlesworth, *Genet. Res.* **55**, 199 (1990).
5. R. S. Howard, *Theor. Popul. Biol.* **45**, 313 (1994).
6. P. D. Keightley and A. Eyre-Walker, *Genetics* **153**, 515 (1999).
7. M. Lynch *et al.*, *Evolution* **53**, 645 (1999).
8. A. S. Kondrashov and J. F. Crow, *Hum. Mutat.* **2**, 229 (1993).
9. A. Eyre-Walker and P. D. Keightley, *Nature* **397**, 344 (1999).
10. Calculation of M and U. Homologous DNA sequences were collected from Genbank for several pairs of species using Entrez (www.ncbi.nlm.nih.gov/Entrez/). Species were chosen for which estimates of the evolutionary divergence date were available from the literature that were not based on a global molecular clock. For mouse/rat, we used the data set described in W. Makalowski and M. S. Boguski [*Proc. Natl. Acad. Sci. U.S.A.* **95**, 9407 (1998)]. Sequences were aligned as described in (9). For each pair of genes, we calculated the rates of synonymous and nonsynonymous substitution. To calculate the rate of synonymous substitution, we only used codons that did not differ by a nonsynonymous substitution. We estimated the rate of transition (K_{ts4}) and transversion (K_{tv}) substitution at fourfold degenerate codons using the method of K. Tamura [*Mol. Biol. Evol.* **9**, 678 (1992)], and the rate of transition (K_{ts2}) substitution at twofold degenerate codons using the method of M. G. Bulmer, K. H. Wolfe, and P. M. Sharp [*Proc. Natl. Acad. Sci. U.S.A.* **88**, 5974 (1991)]. These methods take into account base composition bias. For each gene, we then calculated an overall rate of synonymous transition substitution (K_{ts}) by taking a weighted (by the number of sites) average of the two- and fourfold transition rates, and an overall rate of synonymous substitution (K_s) by summing K_{ts} and K_{tv}. The nonsynonymous substitution rate per codon was calculated as $K_n = -ln(1 - P_n)$, where P_n is the proportion of amino acids that differ between the two sequences. For each pair of homologous sequences, we calculated the average proportion of transitions (N_{ts}) and transversions (N_{tv}) that would change an amino acid. The genomic amino acid (M) and deleterious (U) mutation rates were calculated as $M = Z(K_{ts}N_{ts} + K_{tv}N_{tv})$, and $U = M - Z\bar{K}_n/3$, where averages were unweighted averages across genes and Z is a constant that converts the per site estimate to a per genome per generation estimate: e.g., for human/chimpanzee, $Z = 2$(genomes) $\times$ 80,000 (genes) $\times$ 1500 (base pairs for a gene) $\times$ 25 (years for a generation)/[12 $\times$ 10⁶ (years of divergence)]. In the *D. melanogaster/D. pseudoobscura* comparison, we restricted our analysis to genes that were greater than 500 base pairs (bp) in length, since the divergence was relatively high (Table 1), and synonymous sites were close to saturation, leading to difficulty in accurately inferring K_{ts}; unfortunately, we were still unable to estimate K_{ts} for two genes, *G6PD2* and *tpi*; these genes were not analyzed.
11. The synonymous substitution rate is correlated to the level of synonymous codon bias in some *Drosophila* species. This may be due to selection on synonymous codon use or a downward bias in the methods used to correct for multiple hits in sequences with high codon bias. To correct our mutation rate estimates, we calculated the average (across the two species) χ_L value for each gene, where χ_L is the departure from expected codon usage assuming no codon bias calculated as a weighted χ^2 statistic [D. C. Shields, P. M. Sharp, D. G. Higgins, F. Wright, *Mol. Biol. Evol.* **5**, 704 (1988)], summed over amino acids, assuming an empirical genomic G and C base content of 40%. We then regressed the estimates of M and U obtained from each gene against the average χ_L value taking the y intercepts as our corrected M and U values; these are the predicted values of M or U for no synonymous codon bias.
12. H. Akashi, *Genetics* **139**, 1067 (1995).
13. J.-J. Jaeger, H. Tong, C. Denys, *C. R. Acad. Sci. Paris Ser. II* **302**, 917 (1986).
14. D. Yoder and Z. Yang, *Mol. Biol. Evol.* **17**, 1081 (2000).
15. J. W. Drake, *Ann. N.Y. Acad. Sci.* **870**, 100 (1999).
16. Examples: *Diptera* [G. C. Varley, G. R. Gradwell, M. P. Hassell, *Insect Population Ecology: An Analytical Approach* (Blackwell Scientific, Oxford, 1973)]; parasitoid wasps [T. M. Blackburn, *J. Anim. Ecol.* **60**, 151 (1991)]; planthoppers [R. F. Denno, K. L. Olmstead, E. S. McCloud, *Ecol. Entomol.* **14**, 31 (1989)].
17. D. J. Allan, *Am. Nat.* **110**, 165 (1976).
18. W. G. Chitwood and M. B. Chitwood, *Introduction to Nematology* (University Park Press, Baltimore, MD, 1974).
19. S. A. Shabalina and A. S. Kondrashov, *Genet. Res.* **74**, 23 (1999).
20. M. D. Adams *et al.*, *Science* **287**, 2185 (2000).
21. D. Petrov, E. R. Lozovskaya, D. L. Hartl, *Nature* **384**, 346 (1996).
22. R. Ophir and D. Graur, *Gene* **205**, 191 (1997).
23. Some studies have inferred that the genome-wide rate of transposition in *Drosophila* is as high as 0.4 [S. V. Nuzhdin and T. F. C. Mackay, *Mol. Biol. Evol.* **12**, 180 (1995)], but as X. Maside, S. Assimacopoulos, and B. Charlesworth [*Genet. Res.* **75**, 275 (2000)] argue, the true transposition rate is likely to be below 0.2 if element families that had become activated in individual lines and transposed at unusually high rates are disregarded.
24. B. Charlesworth and C. H. Langley, *Annu. Rev. Genet.* **23**, 251 (1989).
25. G. Bell, *The Masterpiece of Nature* (Univ. of California Press, San Francisco, CA, 1982).
26. M. Steiper *et al.*, personal communication.
27. T. Ohta, *J. Mol. Evol.* **1**, 150 (1972).
28. L. Chao and D. E. Carr, *Evolution* **47**, 688 (1993).
29. S. A. West, C. M. Lively, A. F. Read, *J. Evol. Biol.* **12**, 1003 (1999).
30. M. Goodman *et al.*, *Mol. Phylogenet. Evol.* **9**, 585 (1998).
31. R. L. Carroll, *Vertebrate Paleontology and Evolution* (Freeman, New York, 1988).
32. R. C. Fleisher, C. E. McIntosh, C. L. Tarr, *Mol. Ecol.* **7**, 533 (1998).
33. J. R. Powell and R. DeSalle, *Evol. Biol.* **28**, 87 (1995).
34. F. Antequera and A. Bird, *Proc. Natl. Acad. Sci. U.S.A.* **90**, 11995 (1993).
35. Supplementary material is available at www.sciencemag.org/feature/data/1053250.shl
36. C. G. Sibley and J. E. Alquist, *Phylogeny and Classification of Birds* (Yale Univ. Press, New Haven, CT, 1990).
37. We thank A. Peters, J-L. Hartenberger, W. Hill, J. Crow, J. Peck, S. West, and S. Otto for helpful discussions and comments, and N. Smith for the data set of mouse/rat genes. Supported by the U.K. Royal Society.

19 June 2000; accepted 24 August 2000

Localized Rac Activation Dynamics Visualized in Living Cells

Vadim S. Kraynov,[1]* Chester Chamberlain,[1]* Gary M. Bokoch,[1,2] Martin A. Schwartz,[3] Sarah Slabaugh,[1] Klaus M. Hahn[1]†

Signaling proteins are thought to be tightly regulated spatially and temporally in order to generate specific and localized effects. For Rac and other small guanosine triphosphatases, binding to guanosine triphosphate leads to interaction with downstream targets and regulates subcellular localization. A method called FLAIR (fluorescence activation indicator for Rho proteins) was developed to quantify the spatio-temporal dynamics of the Rac1 nucleotide state in living cells. FLAIR revealed precise spatial control of growth factor–induced Rac activation, in membrane ruffles and in a gradient of activation at the leading edge of motile cells. FLAIR exemplifies a generally applicable approach for examining spatio-temporal control of protein activity.

Rac is a member of the Ras superfamily of small guanosine triphosphatase (GTPase) proteins (*1*) and plays a critical role in diverse processes, such as control of cell morphology, actin dynamics, transcriptional activation, and apoptosis signaling (*2*). The broad range of events controlled by this GTPase requires regulation of its interactions with multiple downstream targets. The effects of Rac may in part be controlled by regulating the subcellular localization of its activation. GTP exchange factors (GEFs), which regulate nucleotide exchange on Rho GTPases, contain a variety of localization domains and may modulate downstream signaling from Rac (*3*). Rac induces localized actin rearrangements to generate polarized morphological changes (*4*), but it has been difficult to explore how Rac activation produces localized actin behavior in an intact cell. We developed a method based on fluorescence resonance energy transfer (FRET) that quantifies the timing and location of Rac activation in living cells. Here, it was used to study activation of the Rac1 isoform in cell motility and extracellular signal-induced cytoskeletal changes.

Sensing the Rac nucleotide state required introducing a fluorescently labeled biosensor into a cell together with a fusion protein comprising Rac and green fluorescent protein (GFP) (Fig. 1A) (*5*). This protein biosensor was labeled with the acceptor dye Alexa 546, which can undergo FRET with GFP. Because the

Departments of ¹Cell Biology, ²Immunology, and ³Vascular Biology, The Scripps Research Institute, La Jolla, CA 92037, USA.

*These authors contributed equally to this work.
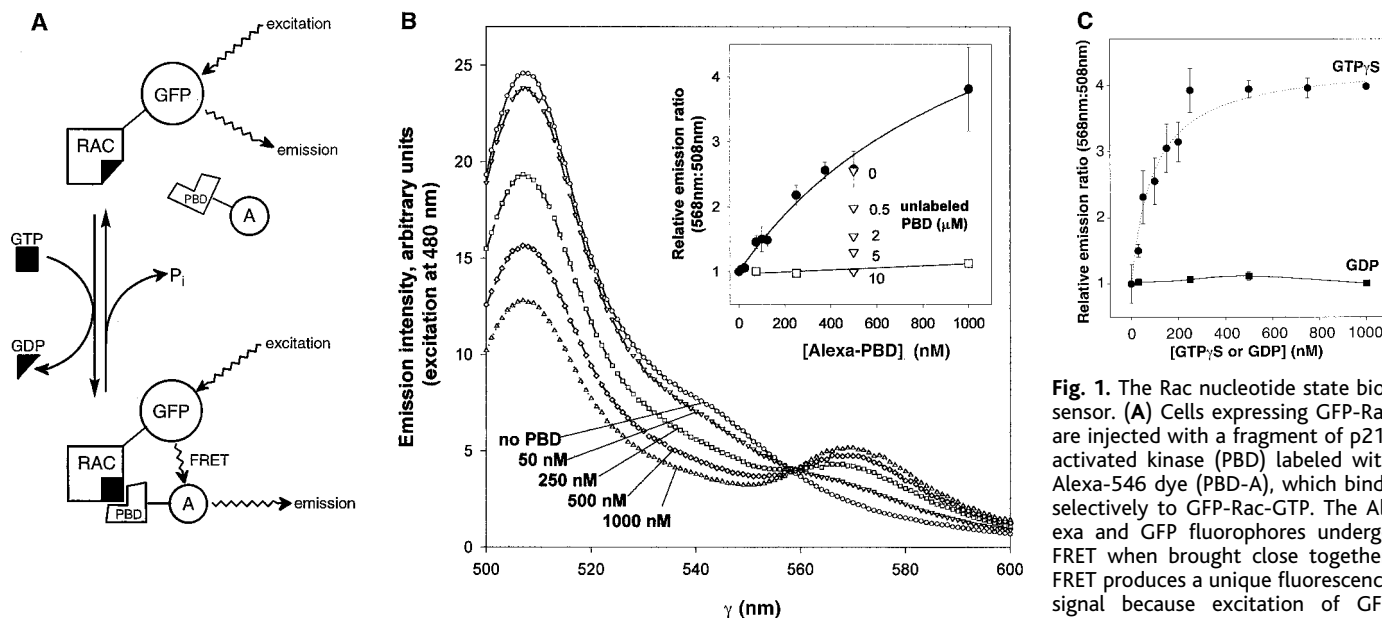†To whom correspondence should be addressed. E-mail: khahn@scripps.edu

Fig. 1. The Rac nucleotide state biosensor. (**A**) Cells expressing GFP-Rac are injected with a fragment of p21-activated kinase (PBD) labeled with Alexa-546 dye (PBD-A), which binds selectively to GFP-Rac-GTP. The Alexa and GFP fluorophores undergo FRET when brought close together. FRET produces a unique fluorescence signal because excitation of GFP leads to emission from Alexa as energy is transferred from the excited GFP fluorophore to the nearby Alexa dye (*30*). This FRET can be measured within a living cell to map the distribution and amount of Rac-GTP binding. By imaging the cell with different wavelengths, both the distribution of Rac and Rac activation can be studied in the same cell. GFP excitation and emission are used for overall Rac distribution, whereas GFP excitation and Alexa emission are used for FRET. (**B**) Fluorescence emission from solutions containing 100 nM GFP-Rac bound to GTPγS at different concentrations of Alexa-PBD. Excitation at 480 nm was used for selective excitation of GFP, and direct (nonFRET) excitation of Alexa was subtracted from these spectra (*9*). In the absence of Alexa-PBD, the emission from GFP (peak at 508 nm) is maximal and no Alexa emission (peak at 568 nm) is observed. Binding of Alexa-PBD to Rac-GFP leads to FRET, producing increasing emission at 568 nm and a decrease at 508 nm. The inset shows variation of the 568-nm/508-nm emission ratio as a function of Alexa-PBD concentration for GFP-Rac bound to GTPγS (circles) or to GDP (open squares). Addition of increasing concentrations of unlabeled PBD blocks FRET (open triangles). (**C**) Variation of this same emission ratio with changes in the nucleotide state of Rac. All data points were the average of three independent experiments.

biosensor was derived from p21-activated kinase 1 (PAK1) (*6, 7*), a specific GTP-Rac target protein, it binds to GFP-Rac only when the Rac is in its activated, GTP-bound form, and produces a localized FRET signal revealing the amount and location of Rac activation. Because the p21-binding domain (PBD) contains no native cysteines, a cysteine residue could be introduced at its NH_2-terminus and then labeled with the cysteine-selective iodoacetamide dye Alexa 546. The distance between the Alexa dye at the NH_2-terminus of PBD and the fluorophore in GFP was calculated to be 52 Å, on the basis of the efficiency of FRET and assuming random rotation of the fluorophores ($R_o = 51$, $n = 1/4$, $k^2 = 2/3$) (*8*). When cells expressing GFP-Rac are injected with the biosensor, the changing location of GFP-Rac and the subpopulation of GFP-Rac molecules in the activated, GTP-bound state can be mapped simultaneously. FRET is proportional to the amount of GTP binding, allowing quantitation of changing activation levels. The name FLAIR (fluorescent activation indicator for Rho proteins) refers to this live-cell imaging technique.

FRET between the purified proteins Alexa-PBD and GFP-Rac in vitro was efficient and dependent on GTP-Rac binding. Using fluorescence excitation wavelengths that selectively excite GFP (480 nm), fluorescence emission was monitored while maintaining a fixed concentration of GFP-Rac and varying Alexa-PBD concentrations (Fig. 1B) (*9*).

Binding of Alexa-PBD to GFP-Rac resulted in a change in fluorescence intensity of both donor (GFP) and acceptor (Alexa) emission. FRET caused the Alexa (acceptor) emission to increase while the GFP (donor) emission decreased. The ratio of emission at these two wavelengths is a sensitive measure of the PBD-Rac interaction. The corrected Alexa/GFP emission ratio (*9*) exhibited a fourfold change upon saturation of Rac with GTP (Fig. 1C). Fluorescence emission changed by <10% when unlabeled PBD or Rac were used under the same conditions (*10*), and competition with unlabeled PBD blocked FRET (Fig. 1B; inset). Change in emission ratio versus PBD concentration was fit to the Michaelis equation to derive an apparent dissociation constant (K_d) for PBD-Rac binding of 1.1 ± 0.3 μM (Fig. 1B, inset), slightly higher than the values determined for various unlabeled PAK1 fragments (*11–13*). The apparent guanosine 5'-O-(3-thiotriphosphate) (GTPγS) dissociation constant was determined at saturating Alexa-PBD by fitting the experimental data to the Michaelis equation (Fig. 1C). The derived value of 47 ± 9 nM is consistent with the previously reported value of 50 nM (*14*). This validated the application of FLAIR as an indicator of biologically relevant Rac-nucleotide binding.

Quiescent Swiss 3T3 fibroblasts that are stimulated with either serum or platelet-derived growth factor (PDGF) initiate membrane ruffling and transcription through activation of Rac (*15, 16*). To monitor the amount and location of Rac activation during this process, the intracellular concentrations of Alexa-PBD and GFP-Rac that altered normal serum-induced ruffle formation were first determined (*17*) (Fig. 2, A and B). Exogenous proteins were added below these concentrations throughout the studies. Image triplets of GFP, FRET, and Alexa fluorescence were taken at each successive time point before and after stimulation (*18*) to simultaneously monitor both the changing localizations of GFP-Rac and the amount and location of Rac activation (Fig. 2, D through F). GFP-Rac fluorescence revealed pools of Rac at the nucleus, in the juxtanuclear region, and in small foci throughout the cell prior to stimulation. Confocal and deconvolution imaging showed nuclear Rac to be concentrated at the nuclear envelope, and expression and immunostaining of epitope-tagged Rac indicated that this localization was not an artifact of GFP tagging (*10*). Addition of PDGF or serum led to formation of moving ruffles containing GFP-Rac throughout the cell periphery within 2 min. The FRET images showed a stark contrast between the amount of Rac activation in the ruffles and the nucleus. No FRET was seen at the nucleus despite the high concentration of Rac there, while the moving ruffles showed the highest FRET, restricted to the ruffle. Thus, Rac activation is
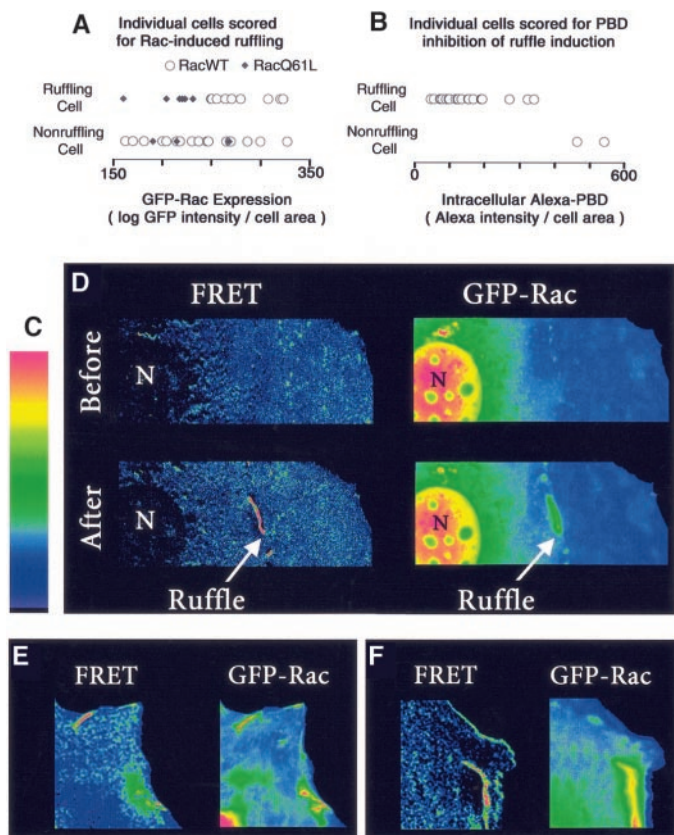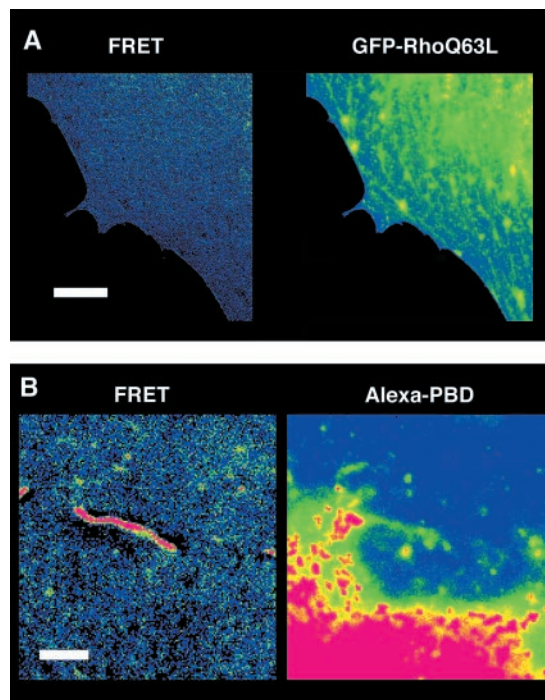
Fig. 2. Rac activation in serum stimulated Swiss 3T3 fibroblasts. (**A**) To determine the amount of GFP-Rac that induces ruffling, quiescent cells expressing different amounts of either wild-type or constitutively active Rac (GFP-Rac Q61L) [amount determined on the basis of (GFP intensity)/(cell area)] were scored for membrane ruffling (*17, 18*). Each point represents an individual cell, placed in the higher (Ruffling) or lower (Nonruffling) row depending on whether ruffling was induced. There is a GFP concentration below which ruffling was consistently not induced by expression of wild-type GFP-Rac. Only cells with Rac expression levels below 250 intensity units on this scale were used in biological experiments. The validity of this approach was supported by scoring of GFP-RacQ61L, which showed ruffle induction at much lower levels of expression. (**B**) To determine the amount of intracellular Alexa-PBD that perturbs normal serum-induced ruffling, cells were scored as in (A). Only cells with Alexa-PBD expression levels below 400 intensity units on this scale were used in biological experiments. (**C**) Color scale for the intensity of FRET or GFP fluorescence for all images. Red represents high and blue is low. The numerical values for the scale are given in the figure legends. (**D**) Rac localization (GFP-Rac) and Rac activation (FRET) before and after stimulation of quiescent Swiss 3T3 fibroblasts with serum (lower images are 3 min after serum addition; cell edge visible to the right and nucleus labeled "N"; bar, 17 μm) (*17, 18*). The cells showed highest accumulation of Rac at and around the nucleus before stimulation (GFP-Rac image). Serum addition generated multiple moving ruffles that showed FRET, whereas no FRET was seen at the nucleus before or after stimulation. Nuclear GFP-Rac associated with the nuclear envelope (see text). In the GFP-Rac images, intensities range between 300 and 1100. The image of FRET before serum addition is scaled to demonstrate the low levels of FRET, with values ranging between 0 and 15. In the image of FRET after stimulation, the ruffle contains the highest values of 40 to 65. (**E** and **F**) Examples of FRET and GFP fluorescence in ruffles. Of 35 cells stimulated with either serum or PDGF, 31 began ruffling within 15 min. FRET was seen in the ruffles of all but one of the ruffling cells. Nuclear FRET was not seen in any of the cells examined.

restricted to the site of actin polymerization, independent of the overall distribution of Rac. Rac activation remained tightly correlated with the position of the ruffle even as it moved throughout the cell (*10*), indicating that structures specifically associated with the ruffle were either binding and concentrating activated Rac or that growth factor–induced Rac activation was specifically localized to ruffles. FRET was also imaged in cells expressing a GFP fusion protein containing a mutant form of Rho, a close relative of Rac that does not bind PBD. This GFP-Rho Q63L mutant, which generates high levels of GTP-bound protein, produced specific Rho localizations but no corresponding FRET signals (Fig. 3A). The function of Rac found at the nuclear envelope remains uncertain, but it may be involved in regulating transcription at times later than those tested here, or may be activated for an unknown role by other stimuli. When activation was concentrated in a small area such as a ruffle, spatially resolved FRET could detect significant activation changes too small to appreciably alter the overall levels of cellular Rac activity. Our data showed that FRET provided much greater sensitivity and selectivity than following Rac activation simply by imaging Alexa-PBD localization (Fig. 3B). FRET produced much lower backgrounds and provided complete selectivity despite the fact that the biosensor can bind to multiple proteins (Alexa-

Fig. 3. Specificity and sensitivity of FLAIR. (**A**) Swiss 3T3 fibroblasts were transfected with GFP-RhoQ36L, a constitutively active mutant of Rho (bar, 22 μm), and cells were prepared and imaged as described for GFP-Rac (*18*), with comparable concentrations of GFP-RhoQ63L and Alexa546-PBD. Despite a constitutively high proportion of GTP-bound protein, the localization of GFP-Rho showed no corresponding FRET. The GFP images show intensities ranging from 10 to 185, while those in the FRET image range from 0 to 10. (**B**) Simple localization of Alexa-PBD is inferior to FRET in quantifying and localizing Rac-GTP binding (bar = 8 μm). The ruffle in Fig. 2D is shown here in close-up, visualized using FRET, or using simple Alexa-PBD localization (*18*). Even though scaling in the Alexa-PBD image is optimized for detection of the ruffle, the high background due to unbound PBD cannot be eliminated, and binding to other target proteins is not eliminated as it is in the highly specific FRET signal. Without prior knowledge of

the ruffle's location, this localization would have been difficult to discern. Color scale for the intensity of FRET or GFP fluorescence is the same as in Fig. 2C.

PBD also binds to cdc42 and other Rac isoforms). Although Alexa-PBD could be sterically hindered from reaching Rac in some locations, a FRET signal in a given location

does reveal that Rac activation is occurring there.

Rac is essential for the directed movement of *Dictyostelium* cells during chemotaxis and

for extension of the cell anterior during motility (*19*). To determine if Rac activation in polarized, motile cells occurred in particular subcellular localizations to regulate localized actin behaviors, FLAIR was applied to a monolayer of confluent Swiss 3T3 fibroblasts in which a wound was scraped, causing cells to become polarized and move into the open space (*20*). FLAIR revealed highest Rac activation in the juxtanuclear area, and a gradient of Rac activity highest near the leading edge and tapering off toward the nucleus (Fig. 4A). The gradient correlated with the direction of cell movement. The difference in Rac activity between the rear of the cell and the leading edge where activity was highest was examined for 16 cells [activity measured in squares 3 μm on a side; percent gradient = 100 × (front − back)/back]. Of 16 cells examined, 12 had higher Rac activity at the leading edge (gradient of 128 ± 51%, mean ± standard error) and four showed a reverse gradient of much smaller magnitude (9 ± 4%). The gradient
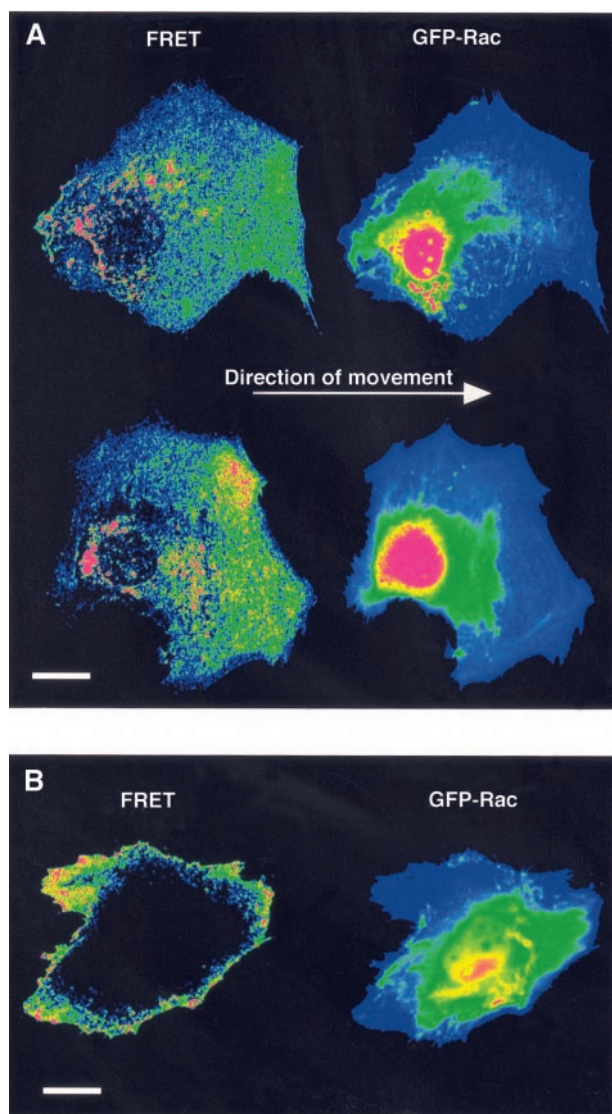
was broader than the narrow area at the leading edge where actin polymerization occurs (*21, 22*). Rac activation over this broad gradient could activate multiple downstream effectors known to be required for motility, to depolymerize fiber networks for monomer recycling or deliver molecules to the leading edge (*22*). Other studies have shown tight localization of molecules downstream of Rac at the leading edge or in regions immediately behind it to regulate a variety of functions associated with motility (*23*). No Rac activation gradient was seen in cells within the monolayer, away from the wound edge. Of 10 cells examined, three showed no discernible FRET, and seven showed FRET around the cell periphery, either in isolated spots (four cells) or uniformly around the edge (three cells, Fig. 4B).

The prevalence of Rac activation around the nucleus was quantified in 16 cells. All cells showed both juxtanuclear and nuclear GFP fluorescence. Of these, 14 showed juxtanuclear

FRET, and none showed nuclear FRET. Notably, small areas of the nucleus sometimes showed a FRET signal, but these could be due either to cytoplasmic Rac associated with the nuclear envelope or to juxtanuclear localizations lying over the nucleus. The localization of activation within the juxtanuclear Rac often did not parallel Rac distribution, with "hot spots" of FRET within areas of lower Rac concentration. The meaning of the juxtanuclear Rac localizations is unclear, but their morphology and distribution suggests activation within the endoplasmic reticulum (ER), golgi, or vesicle populations, consistent with recent reports suggesting an important role for Rac in ER to golgi transport, and in pinocytic vesicle cycling (*2*).

Quantifying the spatial distribution of Rac signaling in living cells indicated that Rac activation was tightly coupled to small membrane ruffles, yet was broadly distributed as a gradient at the leading edge of motile cells. This suggests that the cell uses different distributions of activated Rac to produce specific cellular behaviors. Rac and other GTPases are not simple binary switches, but different kinetics of activation produce profoundly different results (*24*). FLAIR may also be used to examine the kinetics of rapid activation changes, and the approach can potentially be applied to many other types of protein behavior.

Fig. 4. Rac nucleotide state in motile cells. (**A**) Two examples of Rac activation and localization in motile Swiss 3T3 fibroblasts (bar = 24 μm). Cells were induced to move by scraping a wound in a cell monolayer (*20*). The highest concentration of activated Rac1 was seen in the juxtanuclear region, and a gradient of Rac activation was also observed, highest near the leading edge and tapering off toward the nucleus. Color scale for the intensity of FRET or GFP fluorescence is the same as Fig. 2C. FRET intensities are 0 to 18 (top image) and 0 to 32 (bottom image). In the GFP images, intensities range from 98 to 700 (top image) and 100 to 1100 (bottom image). (**B**) Example of a cell in the monolayer, away from the wound. In such cells, FRET was either not detected or found around the cell edge. (GFP intensities = 0 to 1023, FRET intensities = 0 to 10.)

References and Notes

1. A. Hall, *Science* **279**, 509 (1998).
2. L. Kjoller and A. Hall, *Exp. Cell. Res.* **253**, 166 (1999).
3. K. Zhou *et al.*, *J. Biol. Chem.* **273**, 16782 (1998).
4. C. D. Nobes and A. Hall, *J. Cell Biol.* **144**, 1235 (1999).
5. M. C. Subauste *et al.*, *J. Biol. Chem.* **275**, 9725 (2000).
6. PBD of human PAK1 (residues 65 through 150) with a single cysteine added in the penultimate NH$_2$-terminal position, was expressed as a COOH-terminal 6His fusion protein from the pET23 vector (Novagen) and purified from *Escherichia coli* strain BL21DE3 using Talon metal affinity resin (Clontech). All GFP constructs were prepared using the EGFP mutant (*25*). GFP-Rac fusion and wild-type Rac for in vitro studies were also expressed as 6His constructs and purified using a similar procedure. Purified protein was dialyzed against 50 mM sodium phosphate (pH 7.8), and labeled with seven equivalents of Alexa 546 maleimide (Molecular Probes) at 25°C for 2 hours. The conjugate was purified from unincorporated dye by G25 size exclusion chromatography followed by dialysis. The dye:protein ratio was between 0.8 and 1.3, as determined from absorbance of the conjugate at 558 nm (Alexa 546 extinction coefficient 104,000 M^{-1} cm^{-1}) and 280 nm (PBD, extinction coefficient 8250 M^{-1} cm^{-1} plus Alexa absorbance, determined as 12% of the absorbance at 546 nm). Protein concentration was also independently determined using a Coomassie Plus protein assay (Pierce) and SDS-PAGE calibration with known concentrations of bovine serum albumin.
7. V. Benard, B. P. Bohl, G. M. Bokoch, *J. Biol. Chem.* **274**, 13198 (1999).
8. T. K. Nomanbhoy, D. A. Leonard, D. Manor, R. A. Cerione, *Biochemistry* **35**, 4602 (1996).
9. Purified GFP-Rac (200 nM) was bound to varying concentrations of GTPγS or GDP at low magnesium by 30 min incubation at 30°C (*26*), using nucleotide equilibration buffer: 50 mM tris-HCl (pH 7.6), 50 mM NaCl, 5 mM MgCl$_2$, 10 mM EDTA, and 1 mM dithiothreitol. Equal volumes of Alexa-PBD in the same buffer were added to the GFP-Rac solution, and fluorescence emission spectra (500 to 600 nm) were acquired at room temperature and 480 nm excitation. Concentrations

were corrected for twofold dilution upon Alexa-PBD addition. Alexa-PBD concentrations were either varied as shown, or maintained at 1 micromolar when saturating Alexa-PBD was required. The spectra shown were corrected for direct excitation of the Alexa fluorophore by acquiring spectra of Alexa-PBD alone at equivalent concentrations, and subtracting these from spectra shown in Fig. 2. Values for K_d were determined by fitting to the equation: $Y = A*X/(K_d + X)$. Higher, saturating concentrations of Alexa-PBD were not used because errors from subtraction of direct Alexa excitation became larger. The biological activity of GFP-Rac was previously verified (5). The GFP-Rac used for determination of equilibrium constants was shown to be >98% active in binding GTPγS, determined as described (26).

10. C. Chamberlain, data not shown.
11. E. Manser, T. Leung, H. Salihuddin, Z.-S. Zhao, L. Lim, *Nature* **367**, 40 (1994).
12. D. A. Leonard et al., *Biochemistry* **36**, 1173 (1997).
13. G. Thompson, D. Owen, P. A. Chalk, P. N. Lowe, *Biochemistry* **37**, 7885 (1998).
14. L. Menard et al., *Eur. J. Biochem.* **206**, 537 (1992).
15. A. J. Ridley, H. F. Paterson, C. L. Johnston, D. Diekmann, A. Hall, *Cell* **70**, 401 (1992).
16. P. T. Hawkins et al., *Curr. Biol.* **5**, 393 (1995).
17. For serum stimulation experiments, Swiss 3T3 fibroblasts (ATCC, passage 15 through 27) were plated on glass coverslips and then maintained in Dulbecco's modified Eagle's medium (DMEM) with 10% fetal bovine serum (FBS), 1% L-glutamine, and 1% penicillin-streptomycin for at least 24 hours. Media was then replaced with media containing only 0.5% FBS, and cells were maintained for 42 hours. Cells were transfected by microinjecting 200 μg/ml pcDNA-EGFP-Rac plasmid into cell nuclei 2 to 8 hours before the experiment. The EGFP mutant was used in all experiments, cloned and expressed as described (5). Cells expressing the GFP-Rac were then microinjected with 100 mM Alexa-PBD. This concentration produced the appropriate levels of intracellular PBD (Fig. 2B) after the material was diluted when it entered the cells. Cells were mounted in a heated chamber on a Zeiss Axiovert 100TV microscope and maintained in Dulbecco's phosphate-buffered saline (DPBS) (Gibco) to reduce background fluorescence. Cells were then stimulated by replacing the media with DPBS containing 10% FBS or 50 ng/mL PDGF. Images were obtained every 30 s using a Photometrics PXL-cooled CCD camera with 1 × 1 or 3 × 3 binning, and a Zeiss 40× 1.3 NA oil-immersion objective. Fluorescence filters from Chroma were as follows: GFP: HQ480/40, HQ535/50, Q505LP; FRET: D480/30, HQ610/75, 505LP; Alexa: HQ 545/30, HQ 610/75, Q565LP. Cells were illuminated using a 100-W Hg arc lamp. Exposure times for 3 × 3 binning were: GFP, 0.1 s; Alexa-PBD, 0.1 s; and FRET, 0.5 s. For 1 × 1 binning, exposure times were: GFP, 1 s; Alexa-PBD, 1 s, and FRET, 5 s.
18. Images were first background-subtracted and registered to ensure accurate pixel alignment. The GFP-Rac image was then thresholded, changing the intensities of all pixels outside of the cell to zero. Thresholding was based on the GFP image because it had the largest signal-to-noise ratio, providing the clearest distinction between the cell and background. The thresholded GFP-Rac image was used to generate a binary image with all values within the cell = 1 and all outside = 0. The FRET and Alexa-PBD images were multiplied by the binary image, ensuring that the same pixels were analyzed in all three images. Emission appearing in the FRET image from direct excitation of Alexa and GFP was removed by subtracting a fraction of the GFP-Rac and Alexa-PBD images from the FRET image. This fraction depended on the filter set and exposure conditions used. It was determined, as described in detail elsewhere (27), by taking images of cells containing only GFP-Rac or Alexa-PBD alone, and quantifying the relative intensity of emission in the FRET channel and that in the GFP or Alexa-PBD channel. A broad range of intensities was examined and a line was fit to these for accurate determinations. These corrections had to be applied carefully when studying rapidly moving objects such as ruffles. If the ruffle moved between acquisition of the FRET, GFP, or Alexa images, the subtractive correction process would remove light from the FRET image in the wrong place, generating artifactual FRET localizations.

Data from moving features were used only when careful inspection showed the feature to be coincident in the Alexa, GFP, and FRET images, and controls were performed with images taken in different orders. A low-pass filter kernel was applied to the corrected FRET image to remove high-frequency noise (28). Image processing and microscope automation were performed using Inovision ISEE software. Images were contrast stretched and formated for display using Adobe Photoshop software. We tested Rac and PBD fused to GFP mutants that undergo FRET (ECFP and EYFP). Unfortunately, their spectral overlap was more problematic than that of Alexa and GFP, making the corrections described here more difficult. In addition, the GFP mutants showed roughly 25% the FRET of FLAIR. We used FLAIR for these reasons, but the ability to monitor Rac activity simply through protein expression may justify using GFP mutants in some applications.

19. C. Y. Chung, S. Lee, C. Briscoe, C. Ellsworth, R. A. Firtel, *Proc. Natl. Acad. Sci. U.S.A.* **97**, 5225 (2000).
20. For wound-healing experiments, Swiss 3T3 fibroblasts were induced to undergo polarized movement as described (29). The cells were cultured in Dulbecco's modified Eagle's medium (Gibco) supplemented with 10% FBS at 37°C. The cells were trypsinized and then plated on glass coverslips. They were grown to a confluent monolayer and maintained for an additional 3 to 4 days. Cells were then wounded by creating a straight laceration with a sterile razor blade. Cells along the edge of the wound were microinjected with 200 μg/ml pcDNA-EGFP-Rac plasmid DNA. Six hours after the wound was formed, cells expressing the GFP-Rac were microinjected with 100 micromolar Alexa-PBD and allowed ~10 min for recovery. Media was then replaced with DPBS containing 10% FBS to reduce background fluo-

rescence. Images were obtained as described above, using exposure times of 1 s for GFP, 1 s for Alexa-PBD, and 5 s for FRET.

21. Y. L. Wang, *J. Cell Biol.* **101**, 597 (1985).
22. J. A. Theriot and T. J. Mitchison, *Nature* **352**, 126 (1991).
23. F. Michiels et al., *Nature* **375**, 338 (1995).
24. T. Joneson, *Mol. Cell. Biol.* **19**, 5892 (1999).
25. R. Y. Tsien, *Annu. Rev. Biochem.* **67**, 509 (1998).
26. U. G. Knaus, P. G. Heyworth, B. T. Kinsella, J. T. Curnutte, G. M. Bokoch, *J. Biol. Chem.* **267**, 23575 (1992).
27. C. E. Chamberlain, V. Kraynov, K. M. Hahn, *Methods Enzymol.*, in press.
28. K. Castleman, *Digital Image Processing* (Prentice-Hall, Upper Saddle River, NJ, 1996), pp. 207–209.
29. R. DeBiasio, G. R. Bright, L. A. Ernst, A. S. Waggoner, D. L. Taylor, *J. Cell Biol.* **105**, 1613 (1987).
30. J. R. Lakowicz, *Principles of Fluorescence Spectroscopy* (Plenum, New York, 1983), pp. 305–341.
31. The thoughtful comments of M. Symons and C. Waterman-Storer are much appreciated. We thank R. Tsien for providing the EGFP mutant, P. Millman of Chroma for help with filter design, D. Benson and M. Sims of Inovision for help in image analysis and microscope automation, V. Benard for assistance with preparation of PBD, S. Junger for technical assistance, and E. Blanc for expert administrative assistance. For their financial support, we thank NIH (grants R01 GM-57464 and AG15430 to K.M.H. and GM39434 and GM44428 to G.M.B.) and the Arthritis Foundation for a postdoctoral fellowship to V.S.K.

5 June 2000; accepted 25 August 2000

A Myosin I Isoform in the Nucleus

Lidija Pestic-Dragovich,[1]* Ljuba Stojiljkovic,[1]*
Anatoly A. Philimonenko,[2] Grzegorz Nowak,[1] Yunbo Ke,[1]
Robert E. Settlage,[3] Jeffrey Shabanowitz,[3] Donald F. Hunt,[4]
Pavel Hozak,[2] Primal de Lanerolle[1]†

A nuclear isoform of myosin I β that contains a unique 16–amino acid amino-terminal extension has been identified. An affinity-purified antibody to the 16–amino acid peptide demonstrated nuclear staining. Confocal and electron microscopy revealed that nuclear myosin I β colocalized with RNA polymerase II in an α-amanitin– and actinomycin D–sensitive manner. The antibody co-immunoprecipitated RNA polymerase II and blocked in vitro RNA synthesis. This isoform of myosin I β appears to be in a complex with RNA polymerase II and may affect transcription.

Myosin I is a single-headed, nonfilamentous member of the myosin superfamily of actin-based molecular motors (1, 2). There are at least four different subclasses of myosin I proteins, all containing a 110- to 150-kD

[1]Department of Physiology and Biophysics, University of Illinois at Chicago, Chicago, IL 60612, USA. [2]Department of Cell Ultrastructure and Molecular Biology, Institute of Experimental Medicine, Academy of Sciences of the Czech Republic, Prague, Czech Republic. [3]Chemistry Department, University of Virginia, Charlottesville, VA 22901, USA. [4]Departments of Chemistry and Pathology, University of Virginia, Charlottesville, VA 22901, USA.

*These authors contributed equally to this paper.
†To whom correspondence should be addressed. E-mail: primal@uic.edu

heavy chain and one to six light chains. Myosin I is diffusely distributed throughout the cytoplasm (3). It concentrates near cortical surfaces and in the perinuclear region (3), and it appears to mediate plasma membrane extension (3, 4), vesicle and organelle transport (5), and mechanochemical regulation of calcium channels in hair cells (6).

Affinity-purified polyclonal antibodies to bovine adrenal myosin I recognized a 120-kD protein that is larger than the antigen (116 kD) (7). Confocal and electron microscopy showed cytoplasmic and nuclear staining with these antibodies. Biochemical assays on nuclei demonstrated that the 120-kD protein binds adenosine triphosphate (ATP) and calmodulin, is associated with K+-EDTA ATPase activity, and